Check for updates

JGR Atmospheres

RESEARCH ARTICLE
10.1029/2025JD044113

Special Collection:
The Energy Exascale Earth System Model (E3SM): Advancements in a Decade of Earth System Modeling

Evaluating E3SM Global Storm-Resolving Model Simulations of Deep Convection: Insights From DP-SCREAM During TRACER

Raymond Kwaku Twumasi Oware[1,2], Youtong Zheng[1,2], Peter Bogenschutz[3], Yunyan Zhang[3], Hsi-Yen Ma[3], Shaocheng Xie[3], and Cheng Tao[3]

[1]Department of Earth and Atmospheric Science, University of Houston, Houston, TX, USA, [2]Institute of Climate and Atmospheric Science, University of Houston, Houston, TX, USA, [3]Lawrence Livermore National Laboratory, Livermore, CA, USA

Abstract Global Storm-Resolving Models (GSRMs) are becoming increasingly vital for advancing climate modeling and improving the prediction of extreme weather events. Houston, a coastal region frequently affected by deep convective storms, offers an ideal setting to evaluate the ability of GSRMs to simulate deep convection. This study assesses the performance of the Doubly Periodic Simple Cloud-Resolving E3SM (Energy Exascale Earth System Model) Atmosphere Model (DP-SCREAM) using observations from the TRacking Aerosol Convection interactions ExpeRiment (TRACER) campaign. DP-SCREAM effectively reproduces the diurnal cycles of clouds and precipitation, demonstrating much greater skill than the E3SM single column model. The DP-SCREAM is demonstrated to be applicable to coastal regions, partially due to the forcing data sets already capturing the influence of breezes. DP-SCREAM also replicates biases persistent in the global version of SCREAM: the underrepresentation of boundary layer shallow clouds, a lack of mid-level congestus clouds, and the popcorn convection, characterized by small and disorganized convective cells generating the strongest precipitation. To investigate these issues, two sensitivity experiments were conducted: increasing the mixing length and scaling up the buoyancy flux within the Simplified Higher Order Closure scheme. Increasing the mixing length improved mid-level congestus representation and reduced unrealistic early morning fog occurrence. Enhancing buoyancy flux only marginally improved the bias of underproduced big convective cells. An additional resolution sensitivity test at 0.5 km grid spacing demonstrated that a refined horizontal resolution alone is insufficient to resolve these biases.

Plain Language Summary This study evaluates a high-resolution weather model, DP-SCREAM, to assess its ability to simulate storm systems over Houston. The model successfully captures key features such as cloud structures, precipitation, and sea-breeze patterns. However, it consistently exhibits three notable biases: an underrepresentation of middle-level clouds, excessive early morning fog formation, and overproduction of small cells rather than larger systems. To address these issues, adjustments were made to how the model represents atmospheric mixing and buoyancy. Enhancing atmospheric mixing improved middle-level cloud representation and reduced fog occurrence but had a limited effect on improving the organization of storm systems.

Key Points:

- DP-SCREAM simulation captures the diurnal cycles of clouds and precipitation, and sea breeze influences over a coastal region, though some biases remain
- DP-SCREAM simulation can replicate many persistent biases in global SCREAM demonstrating its great value
- Increasing the horizontal resolution of DP-SCREAM does not eliminate key model biases

Supporting Information:

Supporting Information may be found in the online version of this article.

Correspondence to:

Y. Zheng,
yzheng29@central.uh.edu

Citation:

Oware, R. K. T., Zheng, Y., Bogenschutz, P., Zhang, Y., Ma, H.-Y., Xie, S., & Tao, C. (2025). Evaluating E3SM global storm-resolving model simulations of deep convection: Insights from DP-SCREAM during TRACER. *Journal of Geophysical Research: Atmospheres*, *130*, e2025JD044113. https://doi.org/10.1029/2025JD044113

Received 23 APR 2025
Accepted 3 OCT 2025

Author Contributions:

Conceptualization: Youtong Zheng
Data curation: Raymond Kwaku Twumasi Oware, Shaocheng Xie, Cheng Tao
Formal analysis: Raymond Kwaku Twumasi Oware, Youtong Zheng
Funding acquisition: Youtong Zheng
Investigation: Raymond Kwaku Twumasi Oware, Youtong Zheng, Peter Bogenschutz, Yunyan Zhang
Methodology: Raymond Kwaku Twumasi Oware, Youtong Zheng, Shaocheng Xie, Cheng Tao

© 2025. American Geophysical Union. All Rights Reserved.

1. Introduction

Traditional General Circulation Models (GCMs) generally operate at resolutions of several hundred kilometers, requiring the parameterization of deep convection (Arakawa, 2004; Arakawa & Schubert, 1974; Freitas et al., 2020). Recent advancements in computational power and model development have enabled the emergence of Global Storm-Resolving Models (GSRMs), which explicitly simulate deep convection, eliminating the need for parameterization of deep convection (Caldwell et al., 2021; Judt, 2018; Merlis et al., 2024; Randall et al., 2003; Satoh et al., 2019; Stevens & Bony, 2013; Stevens et al., 2019; Takasuka et al., 2024; Tomita et al., 2005). The concept of developing GSRMs was pioneered by Taroh Matsuno (2016), ultimately leading to the creation of the first global non-hydrostatic model called the Nonhydrostatic Icosahedral Atmospheric Model (NICAM) (Satoh et al., 2008, 2014; Stevens et al., 2019; Tomita et al., 2005). NICAM demonstrated that tropical convective storms could be directly represented within the general circulation by solving the unfiltered atmospheric motion equations on a global scale (Stevens et al., 2019). Following NICAM's success, various research groups leveraged increasing computational power to develop additional GSRMs with the shared goal of

21698996, 2025, 20, Downloaded from https://agupubs.onlinelibrary.wiley.com/doi/10.1029/2025JD044113 by Youtong Zheng - University Of Houston Library , Wiley Online Library on [27/10/2025]. See the Terms and Conditions (https://onlinelibrary.wiley.com/terms-and-conditions) on Wiley Online Library for rules of use; OA articles are governed by the applicable Creative Commons License

Project administration: Youtong Zheng
Resources: Youtong Zheng, Yunyan Zhang
Software: Raymond Kwaku Twumasi Oware, Peter Bogenschutz
Supervision: Youtong Zheng
Validation: Raymond Kwaku Twumasi Oware
Visualization: Raymond Kwaku Twumasi Oware
Writing – original draft: Raymond Kwaku Twumasi Oware, Youtong Zheng
Writing – review & editing: Raymond Kwaku Twumasi Oware, Youtong Zheng, Peter Bogenschutz, Yunyan Zhang, Hsi-Yen Ma, Shaocheng Xie, Cheng Tao

overcoming the limitations of deep convection parameterization in traditional GCMs (Randall et al., 2003; Satoh et al., 2019; Stevens & Bony, 2013).

GSRMs use horizontal grid resolutions of 1–5 km, enabling them to capture key atmospheric processes, such as the organization of tropical convection and regional precipitation patterns over complex terrains, with much greater fidelity than traditional GCMs (Bogenschutz et al., 2024; Caldwell et al., 2021; Stevens et al., 2019; Takasuka et al., 2024; Zhang et al., 2024). One of the major advancements in GSRMs is their improved representation of the precipitation diurnal cycle (Ma et al., 2022; Song et al., 2024). While many conventional GCMs incorrectly simulate peak precipitation around noon, observations indicate that it typically occurs in the late afternoon or evening (Caldwell et al., 2021; Christopoulos & Schneider, 2021; Collier & Bowman, 2004; Covey et al., 2016; Dai, 2001, 2006; Dai et al., 1999, 2007; Kousky, 1980; Lee & Wang, 2021; Tang et al., 2021; Tao et al., 2024; Watters et al., 2021). While progress has been made in how convective parameterizations handle trigger, closure, and cold pools (Rio et al., 2009; Xie et al., 2019), persistent biases remain. GSRMs capture this delayed peak and the propagation of convective systems over both land and ocean (Song et al., 2024). Furthermore, the DYAMOND intercomparison project has demonstrated that multiple GSRMs, including NICAM, Icosahedral Nonhydrostatic Model (ICON), and Finite-Volume Cubed-Sphere Model (FV3), show remarkable consistency with observations in reproducing the amplitude, phase, and propagation characteristics of the diurnal precipitation cycle, outperforming traditional climate models (Ma et al., 2022; Stevens et al., 2019). However, the computational cost of running GSRMs remains a major limitation, restricting simulations to relatively short durations, typically 1 month to a year (Caldwell et al., 2021). The high computational demands of GSRMs present challenges for refining these models, but alternative cost-effective configurations may offer opportunities for continued advancements (Donahue et al., 2024; Stevens et al., 2019).

One recent GSRM is the Simple Cloud-Resolving E3SM (Energy Exascale Earth System) Atmosphere Model (SCREAM) developed by the U.S. Department of Energy (Caldwell et al., 2021) which runs at a default 3.25 km resolution. As a cost-effective alternative, the Doubly Periodic configuration of SCREAM (DP-SCREAM) serves as a simplified proxy for high-resolution global SCREAM simulations (Bogenschutz et al., 2023). DP-SCREAM was developed to simulate small regions of the atmosphere with periodic boundary conditions in both horizontal dimensions. It enables efficient high-resolution atmospheric simulations using a single-point 3-D cloud-resolving model on a planar grid with adjustable domain size and resolution. At horizontal resolutions of 1–5 km, DP-SCREAM consistently displays scale insensitivity, but when resolutions get closer to those found in large eddy simulations, sensitivity increases, particularly in the shallow convective regimes (Bogenschutz et al., 2023).

The primary objective of this paper is to introduce and evaluate a new DP-SCREAM case scenario utilizing observations from the TRacking Aerosol Convection interactions ExpeRiment (TRACER) campaign. This modern observational case provides an opportunity to investigate the following research questions:

1. How effective is DP-SCREAM, which assumes a homogeneous surface, in representing convection over coastal regions characterized by significant surface inhomogeneity?
2. To what extent can DP-SCREAM replicate known biases present in the global SCREAM model, such as the lack of mid-level congestus clouds, the popcorn convection issue, and the underrepresentation of shallow clouds?
3. Does refining horizontal resolution help alleviate these biases?

Rather than focusing on individual events, such as the recent study of Bogenschutz, Zhang, et al. (2025), this study uses month-long simulations to robustly document and analyze the statistical behavior of simulated convection during the warm season of Houston. Details about the data for evaluation, models implemented, and a description of experimental design are provided in Section 2. Section 3 presents the results broken into the performance of DP-SCREAM, influences of boundary layer parameterization, and exploring the resolution sensitivity of DP-SCREAM. Conclusions follow in Section 4.

2. Data and Methodology

2.1. Observations

The TRACER field campaign focuses on how aerosol properties influence convective cloud life cycles, particularly in the context of Houston's unique urban and industrial emissions from October 2021 to September 2022 (Jensen, 2019). Our study focuses on the TRACER Intensive Operational Period (IOP) which took place from

21698996, 2025, 20, Downloaded from https://agupubs.onlinelibrary.wiley.com/doi/10.1029/2025JD044113 by Youtong Zheng - University Of Houston Library , Wiley Online Library on [27/10/2025]. See the Terms and Conditions (https://onlinelibrary.wiley.com/terms-and-conditions) on Wiley Online Library for rules of use; OA articles are governed by the applicable Creative Commons License

June–September 2022. These 4 months were selected to capture peak convective events using the ARM Mobile Facility (AMF1), the second-generation C-band Scanning ARM Precipitation Radar, and ancillary instruments such as radiosondes and aerosol measurements (Jensen, 2019).

Cloud properties were evaluated using hourly averaged cloud fraction and liquid water path (LWP) data from the ARM Best Estimate Cloud Radiation (ARMBECLDRAD) product (Xie et al., 2010) whilst surface precipitation was assessed with the ARM constrained variational analysis (VARANAL) product (Xie et al., 2004; Xie & Tao, 2021a; Zhang et al., 2001). The ARMBECLDRAD product has 596 levels ranging from 0.16 to 18.01 km whilst the VARANAL data set has 40 levels ranging from 1,025 to 50 hPa. Both VARANAL and ARM-BECLDRAD products have an hourly temporal resolution. Although TRACER offers surface precipitation data from a rain gauge, it is limited to a single-point location, making it unsuitable for precipitation cell tracking, which requires spatial coverage. To overcome this limitation, we utilized quantitative precipitation estimates derived from the NOAA Multi-Radar/Multi-Sensor (MRMS) data sets (Zhang et al., 2016), offering data at a 1 km horizontal resolution and a 15-min temporal resolution. MRMS combines information from multiple radar sources and sensors, generating high-resolution gridded precipitation data ideal for capturing the spatial and temporal dynamics of precipitation cells. For consistency with our model simulations, we regridded the MRMS precipitation to 3 km resolution.

Despite the value of these observational data sets for model evaluation, they contain uncertainties that should be acknowledged. The ARMBECLDRAD suffers from a reflectivity calibration uncertainty of ±3 dBZ from the Ka-band ARM Zenith Radar (KAZR) (Widener et al., 2012). During TRACER, KAZR reflectivity exhibited losses of up to 10 dB relative to the Radar Wind Profiler (RWP) during sustained rainfall. This discrepancy persisted even as rainfall intensity decreased, suggesting that the loss was due to wet-radome effects rather than hydrometeor attenuation (Feng et al., 2024). The accuracy of the VARANAL data set depends on the quality of field measurements. Uncertainties arising from instrument and measurement errors, as well as scale aliasing and sampling biases, can propagate into the derived dynamical fields or result in missing values (Tang et al., 2019).

2.2. Models

2.2.1. Doubly Periodic SCREAM

The development of SCREAM is supported by the US Department of Energy (DOE) with the goal of developing computationally intensive climate science (Caldwell et al., 2021). In SCREAM, the transportation of elements is handled by the new nonhydrostatic version of the High Order Method Modeling Environment (HOMME-NH) (Dennis et al., 2005, 2012; Evans et al., 2013). HOMME-NH solves the nonhydrostatic equations of motion in a rotating reference frame using the shallow atmosphere approximation (Caldwell et al., 2021). The Simplified Higher-Order Closure (SHOC) scheme is responsible for turbulence and mixing parameterization, which plays a critical role in cloud formation and evolution (Bogenschutz & Krueger, 2013). SHOC uses the double-Gaussian probability density function to compute subgrid-scale liquid clouds and turbulence (Bogenschutz et al., 2023). SCREAM's microphysics is based on the Predicted Particle Properties (P3) scheme of Morrison and Milbrandt (2015) whilst the gas optical properties and radiative fluxes are computed using the RTE (Radiative Transfer for Energetics) + RRTMGP (Rapid Radiative Transfer Model for GCMs, Parallel version) (Pincus et al., 2019). A comprehensive description of the model physics used in these simulations is provided in Caldwell et al. (2021).

The doubly periodic version of SCREAM uses the same physics and dynamics as the global configuration. The only difference here is that the dynamical core is configured on a Cartesian planar grid instead of a spherical grid where surface type, topography, and forcing are across the homogeneous domain (Bogenschutz et al., 2023). DP-SCREAM reads forcing files derived from measurements including initial sounding, large-scale forcing, and surface fluxes. After specifying the latitude and longitude, the surface type is determined by searching the closest grid in the E3SM domain files. Users can adjust key configuration options such as domain size, spatial and temporal resolutions, location and magnitude of spin-up perturbation, and nudging relaxation time scale in a name list file.

In this study, we use DP-SCREAMv0, which is based on the original Fortran implementation of SCREAM. Although SCREAM has since been ported to C++/Kokkos to support GPU acceleration (SCREAMv1; Donahue

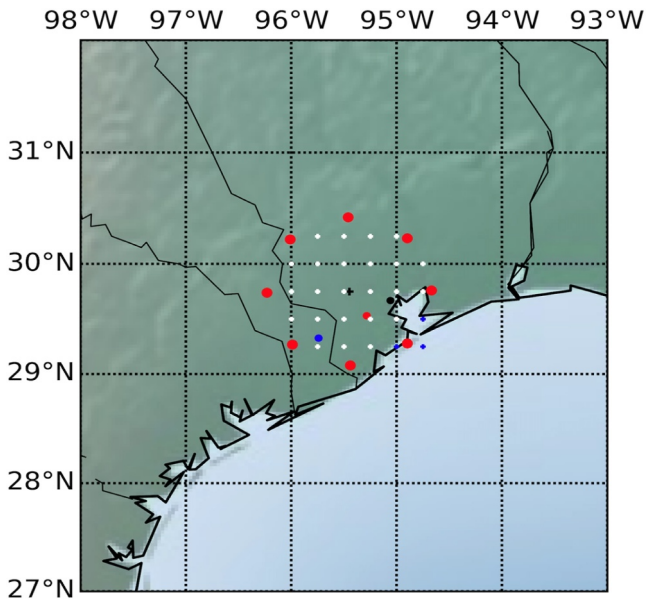


Figure 1. A 75 km radius (bigger red dots) v1 land-only domain with a black cross center. White crosses represent the ERA5 grid that was used to calculate the domain-mean values. Blue crosses in the southeast corner represent the ERA5 grid over the ocean which is not included. Blue, smaller red, and black dots within the 75 km radius represent the TRACER secondary ARM site, TRACER precipitation radar site, and TRACER main ARM site, respectively. The broader domain (98–93°W, 27–32°N) provides geographic context, whereas all analyses in this study employ the 75-km radius v1 land-only domain as forcing to drive DP-SCREAM and the SCM.

et al., 2024), the recently released DP-SCREAMv1 (Bogenschutz, Clevenger, et al., 2025) was not yet ready for scientific application at the time this study was conducted.

2.2.2. Single Column Model

We also use the E3SM version 2 (Golaz et al., 2022) Single Column Model (E3SMv2 SCM) (Bogenschutz et al., 2020) as a reference to DP-SCREAM results. Although the SCM and DP-SCREAM have different sets of parameterizations (Bogenschutz, Zhang, et al., 2025), comparing them helps us to observe how the simulations could be improved by explicitly resolving the kilometer-scale motions. The E3SMv2 employs the High Order Method Modeling Environment (HOMME) dynamical core (Dennis et al., 2012) only for the computation of large-scale vertical advection (Bogenschutz et al., 2020). The physics package includes the Cloud Layers Unified by Binormals (CLUBB) parameterization (Bogenschutz et al., 2013; Golaz et al., 2002) for unified representation of atmospheric boundary turbulence and shallow convection, which is paired with the deep convection parameterization developed by Zhang and McFarlane (1995). The Gettelman and Morrison (2015) scheme is used for microphysics and the RRTMG radiative transfer package (Iacono et al., 2008). More details about the E3SM atmosphere model and its cloud and convection related parameterization can be found in Rasch et al. (2019) and Xie et al. (2018), respectively.

2.3. Experiments

The large-scale forcing and initial conditions from version 1 of the ARM constrained variational analysis (VARANAL v1) (Xie et al., 2004; Zhang et al., 2001) were used for driving DP-SCREAM and the Single Column Model. VARANAL v1 was developed using the European Center for Medium-Range Weather Forecasts (ECMWF) Reanalysis, constrained by surface rainfall retrieved from NOAA's Multi-Radar/Multi-Sensor System (MRMS). In our study, the hourly VARANAL v1 data over a 75 km radius centering the TRACER main ARM site (Figure 1) were used as a forcing file and initial conditions to drive DP-SCREAM and the SCM from July 1 to 28 September 2022.

The MRMS precipitation serves as a key constraint in the VARANAL data, directly influencing the advection tendencies of temperature and moisture. This is important for our DP-SCREAM evaluation because, in observations, some weather systems are advected across the analysis domain (200 × 200 km rectangle). The VARANAL data can capture this information through the precipitation field, which is incorporated into the DP-SCREAM simulations. Our focus on the climatological statistics, instead of individual days, can alleviate the issue of random uncertainties from the forcing data.

DP-SCREAM was run at its default resolution of 3 km resolution over a 200 × 200 km domain from 1 July to 28 September 2022. Our analysis focuses on the period starting in July due to data constraints. The VARANAL v1 data set does not include June because the MRMS precipitation observations required for data assimilation were unavailable. We also ran DP-SCREAM at 0.5 km resolution from 5 August to 15 August 2022. Additionally, two sensitivity experiments were performed at 3 km resolution for August, incorporating perturbations to the mixing length and buoyancy fluxes. All cases of the DP-SCREAM run with SCREAM's default 128 vertical resolution (up to ∼3 hPa) centered on the TRACER main ARM site. The simulations are nudged to horizontal winds from the forcing data. Table 1 gives a summary of the simulations. Details of the experiments will be provided in Section 3.

We applied the Tracking and Object-Based Analysis of Clouds (TOBAC version 1.5.3) algorithm to identify and continuously track convective cells and analyze their characteristics, including cell size, area, and diameter (Heikenfeld et al., 2019; Sokolowsky et al., 2023). Precipitation rate was utilized as the tracking variable to identify convective cells exceeding a threshold of 3 mmday^{-1}. In the feature-detection step, we require at least

21698996, 2025, 20, Downloaded from https://agupubs.onlinelibrary.wiley.com/doi/10.1029/2025JD044113 by Youtong Zheng - University Of Houston Library , Wiley Online Library on [27/10/2025]. See the Terms and Conditions (https://onlinelibrary.wiley.com/terms-and-conditions) on Wiley Online Library for rules of use; OA articles are governed by the applicable Creative Commons License

21698996, 2025, 20, Downloaded from https://agupubs.onlinelibrary.wiley.com/doi/10.1029/2025JD044113 by Youtong Zheng - University Of Houston Library , Wiley Online Library on [27/10/2025]. See the Terms and Conditions (https://onlinelibrary.wiley.com/terms-and-conditions) on Wiley Online Library for rules of use; OA articles are governed by the applicable Creative Commons License

Table 1
Summary of DP-SCREAM Simulations Used in This Study

Simulation name	Horizontal resolution (km)	Time period	Physics time step(s)	Dynamics time step(s)	Mixing length scale factor (length_fac) (unitless)	Liquid water flux scale (unitless)	Description
DP-SCREAM 3 km	3.33	1 July 2022–28 September 2022	100	8.33	0.5	1	Control run
DP-SCREAM 3 km_mix_incr	3.33	1 August 2022–31 August 2022	100	8.33	0.1	1	Sensitivity experiment with enhanced boundary layer mixing
DP-SCREAM 3 km_bf	3.33	1 August 2022–31 August 2022	100	8.33	0.5	2	Sensitivity experiment with increased buoyancy flux
DP-SCREAM 0.5 km	0.5	5 August 2022–15 August 2022	15	1.25	0.5	1	High-resolution run with default configuration

Note. The mixing length scale factor (unitless) is applied to the turbulent mixing length in SHOC, which determines the vertical distance over which turbulent eddies transport momentum and scalars. The Liquid Water Flux Scale parameter (unitless) is applied to the vertical flux of cloud liquid water to adjust buoyancy transport in SHOC.

three contiguous pixels above the threshold of 3 mmday^{-1}. During the linking stage, only features that persisted for at least 5 minutes were retained, excluding short-lived artifacts.

3. Results

The results section is organized into three parts. The first part assesses the overall performance of DP-SCREAM during the TRACER IOP period. The second part investigates model biases by conducting targeted experiments, focusing exclusively on August which is representative of the IOP. In the final part, we assess model sensitivity to horizontal resolutions by comparing DP-SCREAM simulations at resolutions of 0.5 and 3 km over a focused 10-day period from 5 August to 15 August 2022.

3.1. Performance of DP-SCREAM—3 km Resolution

3.1.1. Diurnal Cycle

Figure 2 presents the diurnal cycles of cloud fraction, precipitation rates, and LWP for DP-SCREAM 3 km and E3SMv2 SCM, compared with observations from the ARMBECLDRAD and VARANAL data sets. It must be noted that observed cloud fraction is computed as the hourly frequency of cloud detection at the radar site while the model cloud fraction represents cloud fraction averaged over the model grid cell. The observations show a clear progression from shallow convection to deep convection from the morning to the afternoon. DP-SCREAM 3 km captures both shallow clouds and deep convective anvils but underestimates mid-level congestus between 2 and 6 km during the transition. The underrepresentation of mid-level congestus is consistent with a dry bias between 2 and 6 km, where DP-SCREAM 3 km exhibits notably low relative humidity compared with observations (Figure S1b in Supporting Information S1). Similar low bias in mid-level clouds were reported in the global version of SCREAM (SCREAMv0) simulations over other regions such as the Green Ocean Amazon (GoAmazon) field campaign (Tian et al., 2021, 2024) and other GSRMs simulations over tropical regions (Su et al., 2025). The E3SMv2 SCM completely misses the main feature of the cloud cover diurnal cycle (Figure 2b). It captures some shallow and mid-level clouds up to around 8 km, primarily in the morning but fails to capture upper-level anvil clouds.

In addition to mid-level congestus, DP-SCREAM also markedly underestimates the boundary layer shallow cloud fraction (Figure S1a in Supporting Information S1). This underestimation is consistent with the warm and dry bias within the boundary layer (Figure S2 in Supporting Information S1). The missing mid-level congestus and underproduced boundary layer clouds jointly lead to a significant underestimation of LWP (Figure 2d). Observations in Figure 2d display a strong afternoon peak in LWP around 14:00 LT, associated with daytime convection. E3SMv2 SCM exhibits a noticeable peak in the early morning but underestimates LWP in the afternoon. DP-

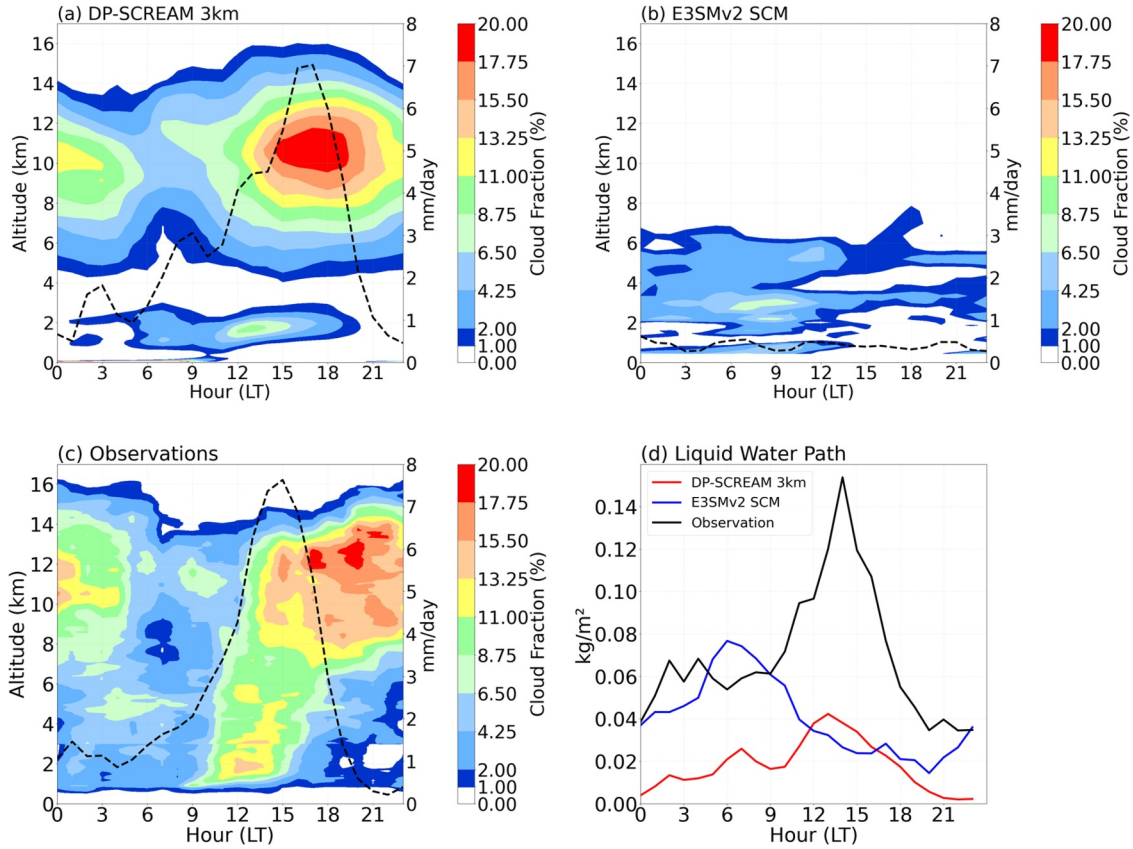


Figure 2. Diurnal Cycle of Cloud Fraction (in contour plots) and Precipitation Rate (in short black dashes) (a–c) and Cloud Liquid Water Path (d) for DP-SCREAM 3 km, E3SMv2 SCM, and observation averaged from 1 July to 28 September 2022.

SCREAM 3 km shows a weaker peak around noon and consistently underestimates LWP throughout the day. Zheng et al. (2024) found similar discrepancies in cloud liquid water path in SCREAMv0 during the marine cold-air outbreaks, where liquid water in mixed-phase cumulus clouds was consistently underestimated.

Regarding precipitation, DP-SCREAM 3 km well reproduces a realistic late afternoon peak (Figure 2a). However, it produces an unrealistic early morning precipitation peak, probably due to excessive fog formation (Figure S1a in Supporting Information S1). The E3SMv2 SCM, as expected, fails to capture the diurnal cycle of precipitation.

3.1.2. Sea Breeze and No Sea-Breeze Days

To understand whether the occurrence of sea breeze influences the performance of DP-SCREAM, we divided the DP-SCREAM 3 km run period into sea-breeze and no sea-breeze days using the classification data sets from Wang et al. (2024). Wang et al. (2024) identified sea-breeze fronts at the TRACER main ARM site based on the presence of front-like signatures in at least three of four data sources: GOES-16 visible reflectance, NEXRAD radar reflectivity, and surface wind direction and moisture from TRACER ground observations. There were 33 days with sea-breeze fronts and 54 days with no sea-breeze influences during the period. However, it should be noted that the classification only captures sea-breeze fronts passing directly over the TRACER main ARM site.

Therefore, it remains possible that there were additional sea-breeze events occurring in the region, which were not detected at the main TRACER ARM site Figures 3a and 3b show the cloud fraction for sea breeze and no sea breeze days in the DP-SCREAM 3 km simulation. Both groups show similar biases of missing mid-level congestus during the transition and the underestimation of boundary layer shallow clouds. The latter bias is more pronounced on no sea-breeze days, as evidenced by lower LWP values shown in Figures 3e and 3f. Wang et al. (2024) show that sea-breeze days are dominated by high-pressure systems over the area, leading to a more

21698996, 2025, 20, Downloaded from https://agupubs.onlinelibrary.wiley.com/doi/10.1029/2025JD044113 by Youtong Zheng - University Of Houston Library , Wiley Online Library on [27/10/2025]. See the Terms and Conditions (https://onlinelibrary.wiley.com/terms-and-conditions) on Wiley Online Library for rules of use; OA articles are governed by the applicable Creative Commons License

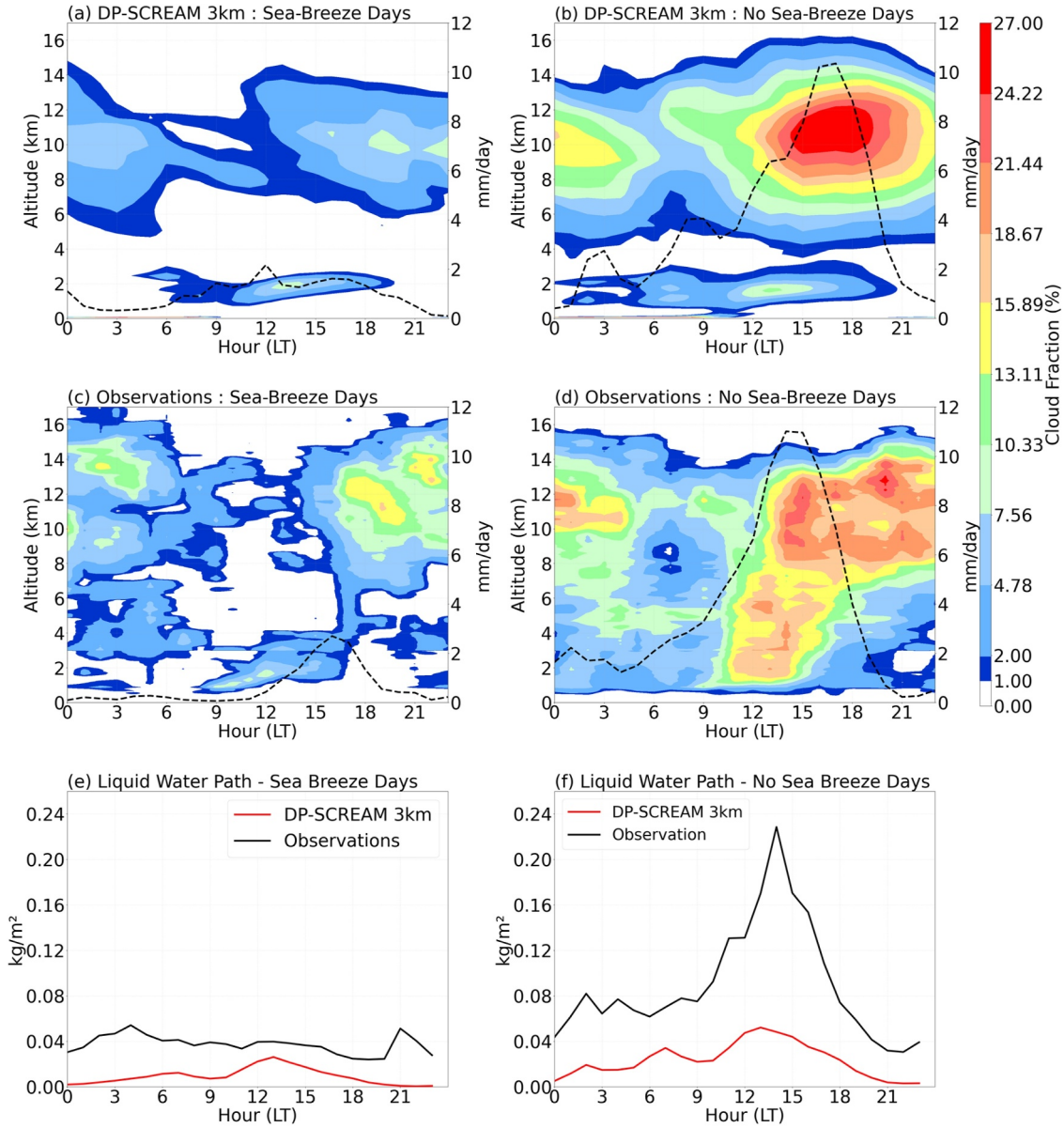


Figure 3. Cloud fraction (shaded, %) and precipitation (black dashed lines) from DP-SCREAM 3 km (panels a, b) and observations (panels c, d) on sea-breeze days (left) versus no sea-breeze days (right). Panels (e, f) show the corresponding diurnal cycles of cloud liquid water path (LWP) for DP-SCREAM 3 km (red) and observations (black).

stable and drier atmosphere. Such a contrast in synoptic environment between sea-breeze and no sea-breeze days is well captured by the TRACER VARANAL forcing data (Figure S3 in Supporting Information S1), allowing DP-SCREAM to simulate weaker convection in sea-breeze days than in no sea-breeze days, consistent with observations. Wang et al. (2024) show that the TRACER main ARM site is markedly influenced by the passages of sea breezes (or bay breeze from Galveston Bay) around 13:00 Local Time (LT), which can enhance boundary layer turbulence that serves as a potential triggering of convection. Since DP-SCREAM cannot explicitly simulate sea breezes, missing such a convection-triggering mechanism might lead to an underestimation of convection during passages of sea breezes at approximately 13:00 LT. Our simulations, however, do not show such a signature on sea breeze days. There are two possibilities. First, the contrast in the synoptic environments between the sea breeze and no sea breeze days is so large that the signals of enhanced triggering by sea breeze are overwhelmed by the synoptic difference. Second, the VARANAL data used to force the model already "feels" these effects from sea breezes. The surface precipitation from the MRMS is an important constraint of the large-

21698996, 2025, 20, Downloaded from https://agupubs.onlinelibrary.wiley.com/doi/10.1029/2025JD044113 by Youtong Zheng - University Of Houston Library , Wiley Online Library on [27/10/2025]. See the Terms and Conditions (https://onlinelibrary.wiley.com/terms-and-conditions) on Wiley Online Library for rules of use; OA articles are governed by the applicable Creative Commons License

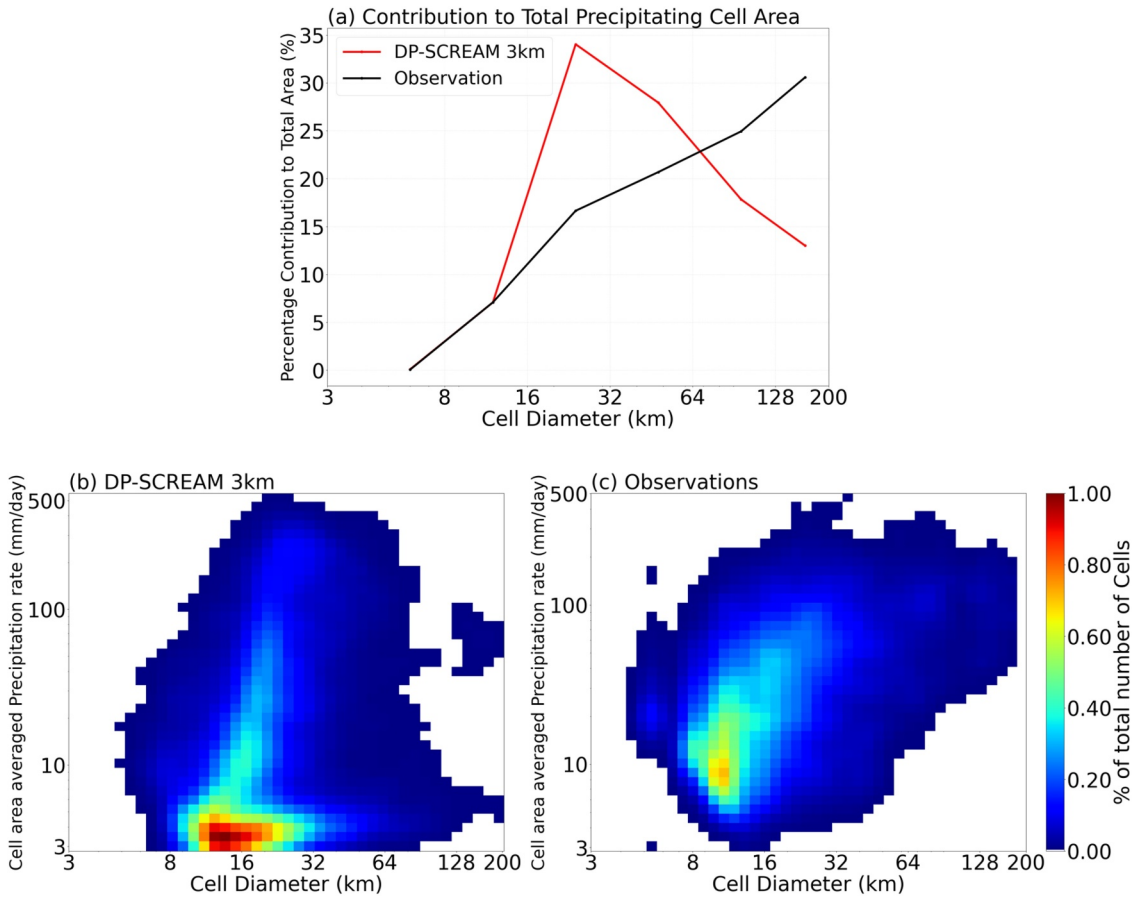


Figure 4. Contribution to Total Precipitating cell area by diameter (a) and 2D-Histogram of cell-averaged precipitation rate (b, c) for DP-SCREAM 3 km and observations from 1 July to 28 September 2022.

scale forcing in the VARANAL data. The impacts of sea breeze on convection are communicated through the precipitation to the forcing fields such as the large-scale vertical velocity and the advections of temperature and moisture.

3.1.3. Precipitation Cluster Statistics

Figure 4a shows the contribution of the total precipitating cell area by the diameter in DP-SCREAM and observation. For observation, we used MRMS precipitation data that were regridded to 3 km resolution and remapped onto a domain consistent with DP-SCREAM. DP-SCREAM 3 km overestimates the contribution of medium-sized precipitating cells (16–32 km) while underrepresenting larger cells compared to observations. This reflects the well-known "popcorn" convection problem, which occurs when GSRMs produces scattered short-lived rain clouds that pop up randomly such as popcorn, instead of forming organized storm systems like we often see in the real atmosphere (Bao et al., 2024; Becker et al., 2021; Caldwell et al., 2021; Crook et al., 2019; Feng et al., 2023). In observations, larger cells produce stronger precipitation (Figure 4c), consistent with the upscale growth process of small and weakly precipitating cells naturally aggregating to form larger cells that produce the strongest precipitation. In DP-SCREAM, however, the strongest rain events happen in small to medium-sized cells (Figure 4b), suggesting an inadequate cell aggregation. The results hold for different thresholds of 1 and 5 mmday^{-1} (Figures S4 and S5 in Supporting Information S1). Moreover, the limited domain size cannot explain the bias because increasing the size to 400 × 400 km yields a similar cell size distribution (Figure S6 in Supporting Information S1).

The lack of upscale growth in DP-SCREAM can be more clearly seen in Figure 5, showing the diurnal progression of precipitation cluster sizes and their contribution to total area in the model (Figure 5a) and observations

21698996, 2025, 20, Downloaded from https://agupubs.onlinelibrary.wiley.com/doi/10.1029/2025JD044113 by Youtong Zheng - University Of Houston Library , Wiley Online Library on [27/10/2025]. See the Terms and Conditions (https://onlinelibrary.wiley.com/terms-and-conditions) on Wiley Online Library for rules of use; OA articles are governed by the applicable Creative Commons License

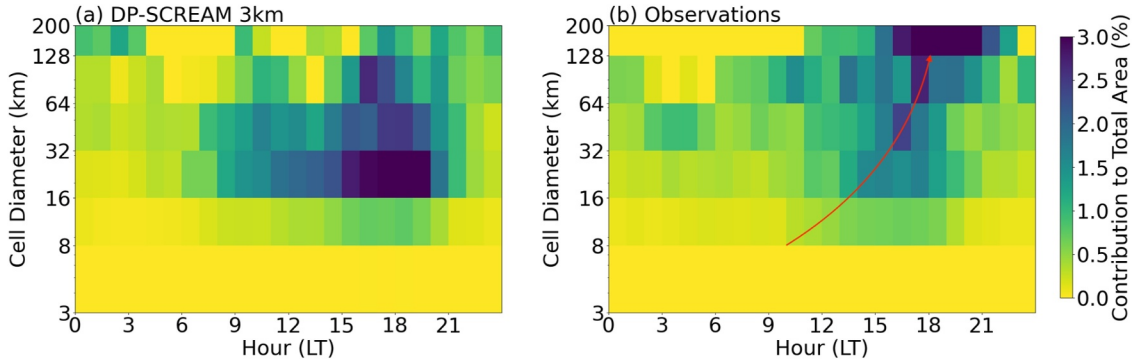


Figure 5. Diurnal cycle of the mean contribution to cell area for (a) DP-SCREAM 3 km and (b) observations from 1 July to 28 September, 2022. The red line in panel (b) shows the upscale growth of cells from morning to the late afternoon.

(Figure 5b). In DP-SCREAM, cluster growth is largely confined to diameters between 16 and 32 km, with peak contributions occurring between 15:00 and 20:00 LT. In contrast, observations demonstrate a distinct upscale growth of convective clusters, consistent with the results shown in Figure 4. This limitation in DP-SCREAM mirrors results from SCREAMv0 during the GoAmazon campaign, where cluster sizes also appeared capped at around 16–32 km (Tian et al., 2024), failing to transition into larger organized systems. The consistency of these findings increases confidence that DP-SCREAM is capable of reproducing some of the biases observed in SCREAMv0, further highlighting the model's limitations in capturing upscale growth dynamics.

Tian et al. (2024) attribute the suppression of upscale growth in SCREAMv0 to the land-atmosphere coupling. Specifically, mid-afternoon precipitation clusters significantly reduce surface incoming shortwave radiation, triggering downward sensible heat transport from the boundary layer to the surface. This energy exchange suppresses sustained convection and aggregation, resulting in the frequent formation of smaller precipitation clusters rather than larger-scale organized convection. In DP-SCREAM, there is no land-atmosphere interaction because surface fluxes, including sensible and latent heat fluxes, are prescribed using VARANAL data. Thus, other factors, such as the inadequate boundary layer parameterization, might contribute to this bias in our simulations.

3.2. Exploring the Influences of Boundary Layer Parameterization

The analyses from the previous section identified four biases in DP-SCREAM: (a) underestimated boundary layer shallow clouds (Figure 2a and Figure S1 in Supporting Information S1), (b) missed mid-level congestus during shallow to deep convection transition (Figure 2a), (c) a lack of upscale growth of convection (Figures 4 and 5), and (d) overproduced early morning fog (Figure S1 in Supporting Information S1).

While we do not aim to comprehensively address all the biases, we focus on the influence of SHOC parameterization in this study. The reasons are twofold. First, a preliminary analysis of early morning fog (see Text S1 in Supporting Information S1) suggests a potential bias of SHOC to undermix the boundary layer, leading to a too-rapid accumulation of moisture near the surface and the unrealistic early morning fog. Artificially enhancing the mixing significantly alleviates this issue (Figure S9 in Supporting Information S1). Second, the coexistence of both underestimated shallow clouds and the absence of mid-level clouds during transition naturally leads one to hypothesize that an insufficient vertical growth of shallow convection will impede the transition from shallow to deep convection (Bogenschutz, Zhang, et al., 2025; Tian et al., 2024). Thus, enhancing the shallow convection might improve the transition simulations.

Drawing from this, we designed two targeted experiments. In the first experiment, DP-SCREAM 3 km_mix_incr, we increased the mixing length in the SHOC parameterization scheme by reducing the mixing length scale factor (length_fac) from its default value of 0.5 to 0.1. This adjustment was motivated by the need to improve the representation of early morning fog and stable boundary layers. Reducing length_fac to 0.1 enhances small-scale vertical mixing in stable conditions, promoting more realistic fog dissipation. In the second experiment, DP-SCREAM 3 km_bf, the magnitude of the liquid water flux $\left(\overline{w'q_l'}\right)$ within the buoyancy flux in SHOC was

21698996, 2025, 20, Downloaded from https://agupubs.onlinelibrary.wiley.com/doi/10.1029/2025JD044113 by Youtong Zheng - University Of Houston Library , Wiley Online Library on [27/10/2025]. See the Terms and Conditions (https://onlinelibrary.wiley.com/terms-and-conditions) on Wiley Online Library for rules of use; OA articles are governed by the applicable Creative Commons License

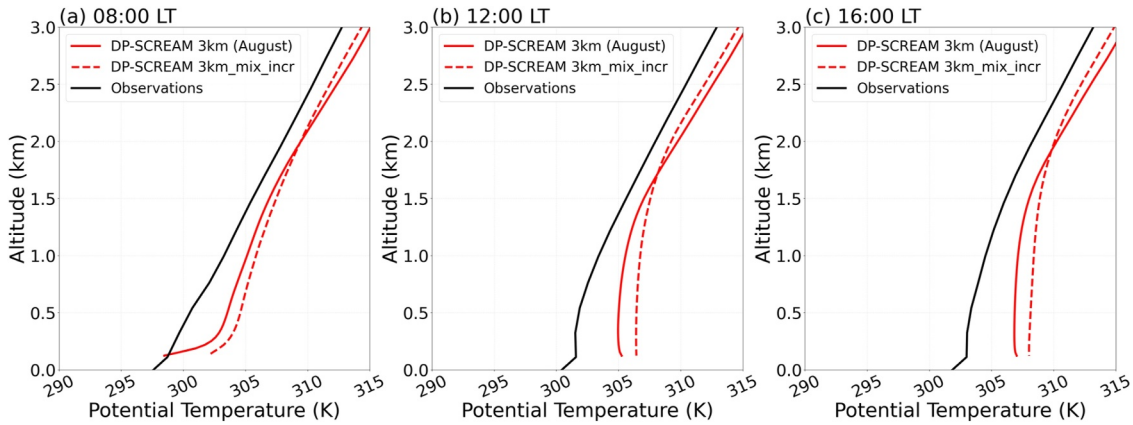


Figure 6. Temporal evolution of potential temperature profiles from DP-SCREAM 3 km (August) resolution (solid red), DP-SCREAM 3 km_mix_incr (dashed red), and observations (black) shown at (a) 08:00 LT, (b) 13:00 LT, and (c) 16:00 LT for August 2022.

increased by a scale factor (χ) of 2 (Bogenschutz, Zhang, et al., 2025). The parameterization of buoyancy flux ($\overline{w'\theta_v'}$):

$$\overline{w'\theta_v'} = \overline{w'\theta_l'} + \frac{1-\epsilon_0}{\epsilon_0}\theta_o\overline{w'q_t'} + \chi\left[\frac{L_v}{C_p}\left(\frac{p_o}{p}\right)^{R_d/C_p} - \frac{1}{\epsilon_o}\theta_o\right]\overline{w'q_l'} \quad (1)$$

includes terms of the liquid water potential temperature flux ($\overline{w'\theta_l'}$) representing the turbulent transport of heat driven by temperature fluctuations; total water flux ($\overline{w'q_t'}$), capturing the turbulent transport of the total water mixing ratio including contributions from both water vapor and liquid water; the liquid water flux ($\overline{w'q_l'}$) which represents turbulent transport specifically to liquid water; ϵ_0 represents ratio of gas constants; and θ_o represents the reference potential temperature.

We run these two sensitivity experiments for August only, a month representative of the overall 3-month simulation period. August exhibits similar diurnal cycles of cloud fraction, comparable distributions in the 2D histograms of cell-averaged precipitation, and importantly, it captures the same key biases relative to observations (Figure S11 in Supporting Information S1) that are similar to the IOP.

The enhanced mixing deepens the boundary layer, as demonstrated in Figure 6, leading to an increase in boundary layer cloud fraction (Figure 7b) as a result of more effective vertical transport of heat and moisture. We observed a significant warm bias in the lower levels of the simulation, similar to our previous 3-month run (Figure S2b in

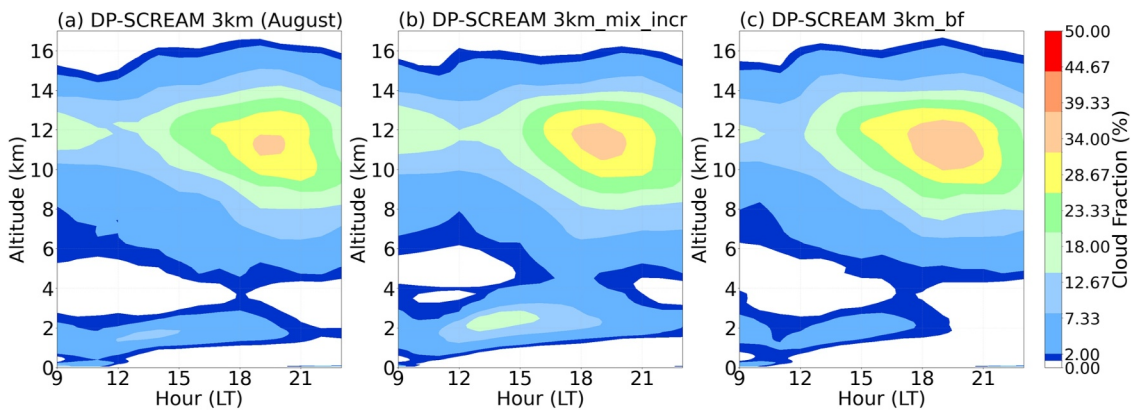


Figure 7. Cloud fraction for (a) DP-SCREAM 3 km (August), (b) DP-SCREAM 3 km_mix_incr, and (c) DP-SCREAM 3 km_bf from 9:00 LT to 23:00 LT during August 2022.

21698996, 2025, 20, Downloaded from https://agupubs.onlinelibrary.wiley.com/doi/10.1029/2025JD044113 by Youtong Zheng - University Of Houston Library , Wiley Online Library on [27/10/2025]. See the Terms and Conditions (https://onlinelibrary.wiley.com/terms-and-conditions) on Wiley Online Library for rules of use; OA articles are governed by the applicable Creative Commons License

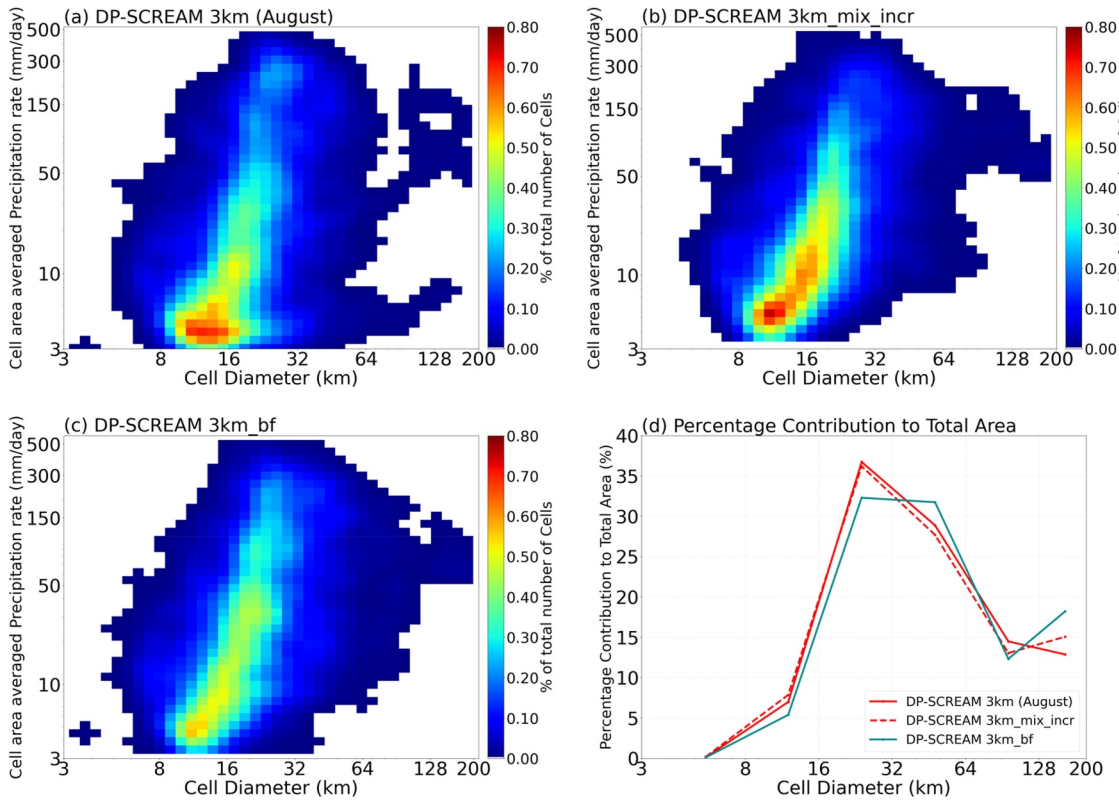


Figure 8. A 2D -Histogram of cell-averaged precipitation rate for DP-SCREAM 3 km (August) (a), DP-SCREAM 3 km_mix_incr (b) and DP-SCREAM 3 km_bf (c), and the Contribution to Total Precipitating cell area by diameter for DP-SCREAM 3 km (August) (solid red), DP-SCREAM 3 km_mix_incr (dashed red), and DP-SCREAM 3 km_bf (solid cyan).

Supporting Information S1), with enhanced mixing further increasing the warm bias in the planetary boundary layer (PBL). While this bias is evident, its impact on the diurnal cycle has not been directly assessed and remains an open question for future study. The improved boundary layer cloud fraction subsequently supports the formation of mid-level congestus clouds, as evidenced by the enhanced cloud representation in Figure 7b (also see Figure S7 in Supporting Information S1).

While there is an improvement in the mid-level congestus, adjusting the mixing length alone does not immediately resolve the "popcorn" convection issue. Figure 8b shows that DP-SCREAM continues to produce a high concentration of small to medium-sized precipitating cells with intense precipitation rates. Although increasing the mixing length slightly enhances the contribution of total precipitating cell area from cells with diameters between 128 and 200 km (which includes 21 cells in this range), it does not fully resolve the underlying bias in the precipitation distribution (Figure 8d).

Previous studies found that increasing the buoyancy flux enhances the vertical representation of shallow convection in SCREAM (Bogenschutz, Zhang, et al., 2025). In the GoAmazon case, adjusting the buoyancy flux improves transition timing in a 1-day simulation. In our month-long climatological analysis of the DP-SCREAM 3 km_bf, we found that while the timing of the transition did not show marked change (Figure 7c), there was an enhancement in the representation of larger precipitating cells contributing to the total precipitating area (Figure 8d). This suggests that while the increase in buoyancy flux had a limited impact on transition timing, it may have marginally improved the distribution of precipitation among different cell sizes.

3.3. Horizontal Resolution Sensitivity

As computational power increases and the resolutions of GSRMs become finer, it is crucial to examine to what extent the same model biases persist in simulations with a finer resolution. To explore the horizontal resolution sensitivity, we conducted a 10-day simulation of DP-SCREAM at a horizontal resolution of 0.5 km

21698996, 2025, 20, Downloaded from https://agupubs.onlinelibrary.wiley.com/doi/10.1029/2025JD044113 by Youtong Zheng - University Of Houston Library , Wiley Online Library on [27/10/2025]. See the Terms and Conditions (https://onlinelibrary.wiley.com/terms-and-conditions) on Wiley Online Library for rules of use; OA articles are governed by the applicable Creative Commons License

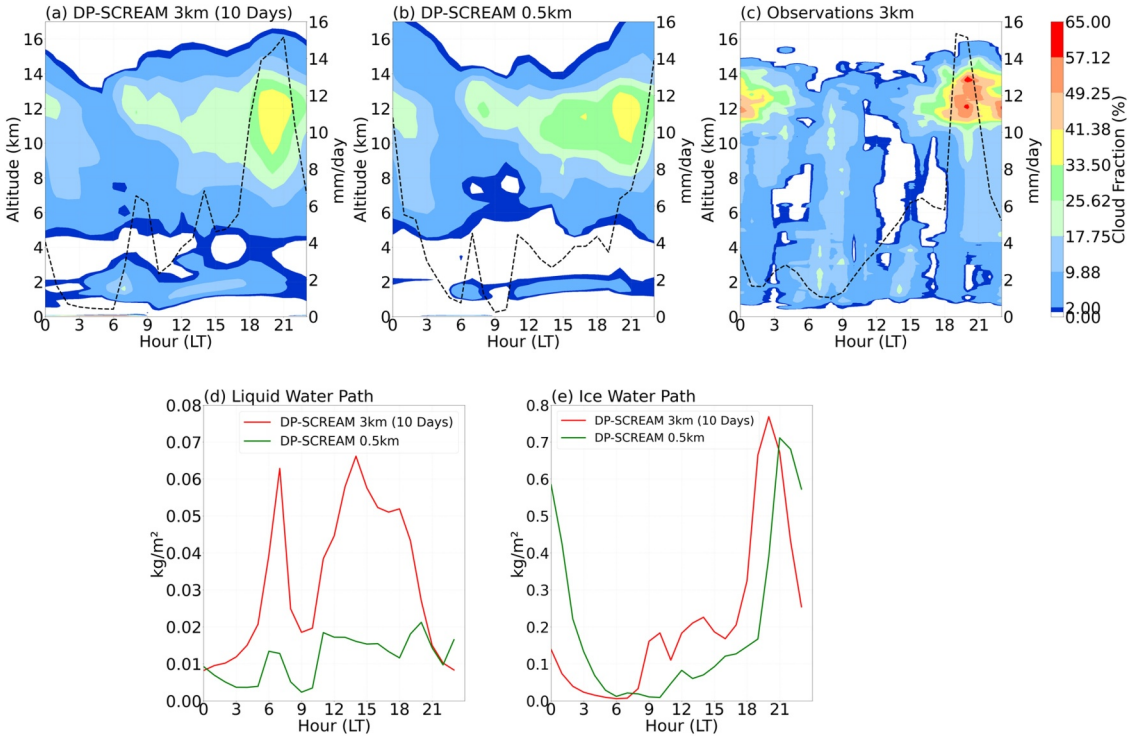


Figure 9. Diurnal cycle of cloud fraction and precipitation rate (black dashes) for DP-SCREAM 3 km (a), DP-SCREAM 0.5 km (b), and observations in 3 km resolution (c). Panels (d, e) show the liquid water path and ice water path, respectively, for DP-SCREAM 3 km (10 Days) and 0.5 km from 5 August to 15 August 2022.

(DP-SCREAM 0.5 km) over a 200 × 200 km domain (Table 1). The simulation period from 5 August to 15 August 2022, was selected to reduce computational cost while still capturing key features representative of the 3-month climatology (Figure S12 in Supporting Information S1). The 0.5 km resolution was selected as it represents the finest horizontal scale achievable within our computational constraints. We acknowledge that model behavior may differ at finer resolutions and should be explored in future work. As shown in Figure 9b, DP-SCREAM 0.5 km produces marginally stronger deep convection but significantly fewer shallow clouds compared to DP-SCREAM 3 km (10 Days) (also see Figure S8 in Supporting Information S1). These findings suggest that boundary layer clouds are sensitive to horizontal resolution changes while deep convective clouds display comparatively lower sensitivity. This contrast is further supported by the pronounced differences in the liquid water path and ice water path shown in Figures 9d and 9e. A similar conclusion was drawn by Bogenschutz et al. (2023), who demonstrated that boundary layer clouds exhibit the greatest sensitivity to resolution during the ARM97 and GATE campaigns. Despite the higher resolution, DP-SCREAM 0.5 km still fails to capture mid-level congestus and continues to produce fog.

In terms of precipitation cluster distribution, the popcorn convection bias persists and worsens in the DP-SCREAM 0.5 km run (Figure 10b). Although the number of larger convective cells slightly increases, the distribution remains heavily skewed toward smaller events, with the highest precipitation rates dominated by these smaller cells. Because smaller cells collectively occupy less total area, the larger cells disproportionately dominate the total precipitating cell area when they do occur (Figure 10d). It is very unrealistic that convective cells with sizes smaller than 10 km can produce precipitation rate >300 mmday^{-1}, which rarely happens in observations over the same region (Tuftedal et al., 2024). The diurnal cycle of precipitation cluster distribution (Figure 11) shows that the DP-SCREAM 0.5 km run fails to capture the observed gradual transition from small to large precipitation cells. A large portion of strong precipitation cells in DP-SCREAM 0.5 km occurs during nighttime and early morning hours, likely associated with long-lived detrained anvil clouds rather than deep convective updrafts (Figure 11).

Prior studies of the idealized simulations of convective self-aggregation (Muller & Held, 2012; Silvestri et al., 2024; Tompkins & Semie, 2017) also suggest that convective cells are less likely to aggregate as the horizontal resolution gets refined below 2 km, particularly under homogeneous initial conditions. Silvestri

21698996, 2025, 20, Downloaded from https://agupubs.onlinelibrary.wiley.com/doi/10.1029/2025JD044113 by Youtong Zheng - University Of Houston Library , Wiley Online Library on [27/10/2025]. See the Terms and Conditions (https://onlinelibrary.wiley.com/terms-and-conditions) on Wiley Online Library for rules of use; OA articles are governed by the applicable Creative Commons License

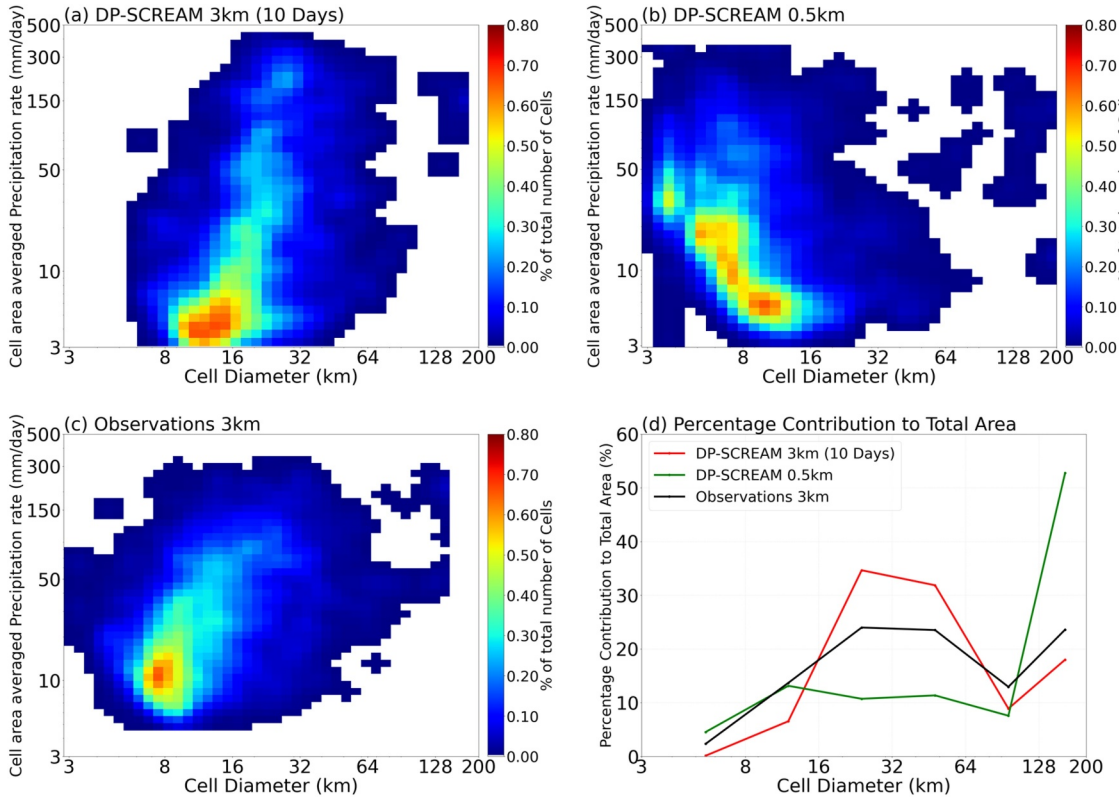


Figure 10. 2D-Histogram of cell-averaged precipitation rate (a–c) and Contribution to Total Precipitating cell area by diameter (d) for DP-SCREAM 3 km (10 Days), DP-SCREAM 0.5 km, and observations in 3 km resolution from 5 August to 15 August 2022.

et al. (2024) argue that numerical diffusion is a key factor controlling the convective upscale growth. As horizontal resolution refines, the numerical diffusion decreases, leading to weaker sensitivity of convective updraft to horizontal entrainment mixing, so that entrainment of dry air into updrafts is ineffective in suppressing updrafts. This significantly weakens the moisture-convection feedback, thus preventing the convective organization. It remains unclear to what degree such a mechanism under an idealized setup of radiative convective equilibrium can explain the worsening of popcorn convection in our simulations in which the large-scale forcing is stronger and the convective cloud clusters are more transient. This is subject to future research.

These results suggest that simply increasing horizontal resolution to 0.5 km is insufficient to resolve the biases in shallow-to-deep convection and precipitation organization. The persistence of these issues points to the crucial role of other physical processes, such as turbulence parameterization and microphysics, in governing cloud evolution and precipitation structure. Further refinement in these areas will be necessary to achieve more realistic simulations.

4. Summary

This study evaluates the performance of the DOE's Simple Cloud-Resolving E3SM Atmosphere Model (SCREAM) using its doubly periodic configuration, DP-SCREAM, to diagnose model biases and test potential improvements in representing deep convection during TRACER. The answers to the three guiding questions posed in the introduction are provided:

1. DP-SCREAM enhances the representation of diurnal cycles of cloud fraction and precipitation, clearly outperforming traditional single-column models relying on parameterized convection. The performance of DP-SCREAM does not degrade on days with reported sea breezes, likely because (a) the forcing data sets effectively capture the synoptic conditions that govern the sea breeze occurrence, and (b) the influence of sea breezes on the convection is encoded in the radar-observed precipitation, which serves as a key constraint in deriving the large-scale forcing.

21698996, 2025, 20, Downloaded from https://agupubs.onlinelibrary.wiley.com/doi/10.1029/2025JD044113 by Youtong Zheng - University Of Houston Library , Wiley Online Library on [27/10/2025]. See the Terms and Conditions (https://onlinelibrary.wiley.com/terms-and-conditions) on Wiley Online Library for rules of use; OA articles are governed by the applicable Creative Commons License

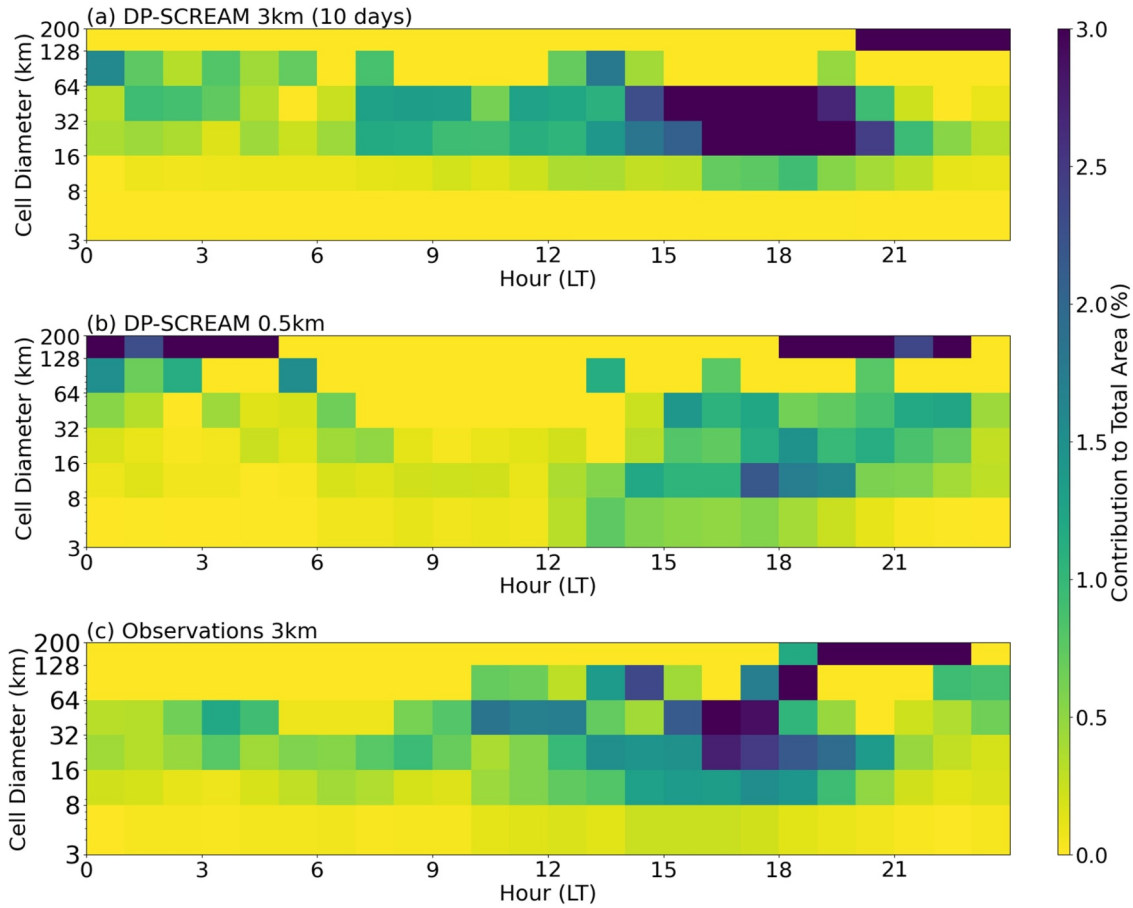


Figure 11. Diurnal Cycle of the mean contribution to cell area for DP-SCREAM 3 km (10 Days), DP-SCREAM 0.5 km, and observations in 3 km resolution from 5 August to 15 August 2022.

2. Despite its strengths, DP-SCREAM replicates several persistent biases commonly observed in global SCREAM simulations. Notably, it underrepresents shallow clouds and mid-level congestus, overproduces mid-size convective cells (with the diameter of several tens of kilometers) that cannot aggregate, and generates unrealistic early morning fog. Targeted sensitivity experiments show that modifying the mixing length and buoyancy flux parameters in SHOC slightly improves the representation of shallow clouds and mid-level congestus but does not fully resolve issues with "popcorn" convection.
3. Increasing the horizontal resolution does not address these biases.

These findings position DP-SCREAM as a strategically valuable testbed for informing SCREAM and guiding its continued development. The VARANAL large-scale forcing plays a crucial role as it provides a meaningful constraint to the simulated system, allowing comparison with the observations despite the doubly periodic idealization. As climate modeling advances toward kilometer-scale resolutions, tools such as DP-SCREAM will be instrumental in accelerating improvements in the representation of convection, clouds, and precipitation across spatial scales and physical regimes. The future work would include testing the influence of cloud microphysical processes on the model biases.

Conflict of Interest

The authors declare no conflicts of interest relevant to this study.

21698996, 2025, 20, Downloaded from https://agupubs.onlinelibrary.wiley.com/doi/10.1029/2025JD044113 by Youtong Zheng - University Of Houston Library , Wiley Online Library on [27/10/2025]. See the Terms and Conditions (https://onlinelibrary.wiley.com/terms-and-conditions) on Wiley Online Library for rules of use; OA articles are governed by the applicable Creative Commons License

Data Availability Statement

Ground based observations during the TRACER field campaign can be accessed and downloaded from DOE ARM's Data Discovery at https://adc.arm.gov/discovery/#/ with a free ARM user account profile. For more details: the VARANAL data set product is available from Xie and Tao (Xie & Tao, 2021b); and ARM Best Estimate Cloud Radiation and liquid water path from Chen and Xie (Chen & Xie, 1996). The MRMS is available at https://www.nssl.noaa.gov/projects/mrms/. The DP-SCREAM and E3SMv2 SCM model output data sets, along with the analysis code used in this study, are publicly available at Zenodo: https://zenodo.org/records/15271730 (Oware, 2025).

Acknowledgments
This work is supported by the DOE Early Career Grant (DE-SC0024185). This research used resources of the National Energy Research Scientific Computing Center (NERSC), a U.S. Department of Energy Office of Science User Facility. Shaocheng Xie and Cheng Tao acknowledge the support from the DOE Atmospheric Radiation Measurement (ARM) program. Peter Bogenschutz, Yunyan Zhang, and Hsi-Yen Ma acknowledge support from the DOE Atmospheric System Research (ASR) program, THREAD project (DOE-SCW1800). Lawrence Livermore National Laboratory is operated by Lawrence Livermore National Security, LLC, for the U.S. Department of Energy, National Nuclear Security Administration under Contract DE-AC52-07NA27344.

References

Arakawa, A. (2004). The cumulus parameterization problem: Past, present, and future. *Journal of Climate*, *17*(13), 2493–2525. https://doi.org/10.1175/1520-0442(2004)017<2493:RATCPP>2.0.CO;2

Arakawa, A., & Schubert, W. H. (1974). Interaction of a cumulus cloud ensemble with the large-scale environment, part I. *Journal of the Atmospheric Sciences*, *31*(3), 674–701. https://doi.org/10.1175/1520-0469(1974)031<0674:IOACCE>2.0.CO;2

Bao, J., Stevens, B., Kluft, L., & Muller, C. (2024). Intensification of daily tropical precipitation extremes from more organized convection. *Science Advances*, *10*(8), eadj6801. https://doi.org/10.1126/sciadv.adj6801

Becker, T., Bechtold, P., & Sandu, I. (2021). Characteristics of convective precipitation over tropical Africa in storm-resolving global simulations. *Quarterly Journal of the Royal Meteorological Society*, *147*(741), 4388–4407. https://doi.org/10.1002/qj.4185

Bogenschutz, P., Zhang, J., Tang, Q., & Cameron-Smith, P. (2024). Atmospheric river induced precipitation in California as simulated by the regionally refined Simple Convection Resolving E3SM Atmosphere Model (SCREAM) version 0. *Atmospheric sciences*. https://doi.org/10.5194/egusphere-2024-839

Bogenschutz, P. A., Clevenger, T. C., Bradley, A., Caldwell, P. M., Beydoun, H., Mahfouz, N., et al. (2025). High performance, high fidelity: A GPU-accelerated Doubly-Periodic version of the Simple Cloud-Resolving E3SM Atmosphere Model version 1 (DP-SCREAMv1). *Preprints*. https://doi.org/10.22541/essoar.174534217.73452258/v1

Bogenschutz, P. A., Eldred, C., & Caldwell, P. M. (2023). Horizontal resolution sensitivity of the simple convection-permitting E3SM atmosphere model in a doubly-periodic configuration. *Journal of Advances in Modeling Earth Systems*, *15*(7), e2022MS003466. https://doi.org/10.1029/2022MS003466

Bogenschutz, P. A., Gettelman, A., Morrison, H., Larson, V. E., Craig, C., & Schanen, D. P. (2013). Higher-order turbulence closure and its impact on climate simulations in the community atmosphere model. *Journal of Climate*, *26*(23), 9655–9676. https://doi.org/10.1175/JCLI-D-13-00075.1

Bogenschutz, P. A., & Krueger, S. K. (2013). A simplified PDF parameterization of subgrid-scale clouds and turbulence for cloud-resolving models. *Journal of Advances in Modeling Earth Systems*, *5*(2), 195–211. https://doi.org/10.1002/jame.20018

Bogenschutz, P. A., Tang, S., Caldwell, P. M., Xie, S., Lin, W., & Chen, Y.-S. (2020). The E3SM version 1 single-column model. *Geoscientific Model Development*, *13*(9), 4443–4458. https://doi.org/10.5194/gmd-13-4443-2020

Bogenschutz, P. A., Zhang, Y., Zheng, X., Tian, Y., Zhang, M., Lin, L., et al. (2025). Exposing process-level biases in a global cloud permitting model with ARM observations. *Preprints*. https://doi.org/10.22541/essoar.173282150.00866424/v1

Caldwell, P. M., Terai, C. R., Hillman, B., Keen, N. D., Bogenschutz, P., Lin, W., et al. (2021). Convection-permitting simulations with the E3SM global atmosphere model. *Journal of Advances in Modeling Earth Systems*, *13*(11), e2021MS002544. https://doi.org/10.1029/2021MS002544

Chen, X., & Xie, S. (1996). Armbecldrad [Dataset]. *Atmospheric Radiation Measurement (ARM) Archive, Oak Ridge National Laboratory (ORNL), Oak Ridge, TN (US); ARM Data Center, Oak Ridge National Laboratory (ORNL)*. https://doi.org/10.5439/1333228

Christopoulos, C., & Schneider, T. (2021). Assessing biases and climate implications of the diurnal precipitation cycle in climate models. *Geophysical Research Letters*, *48*(13), e2021GL093017. https://doi.org/10.1029/2021GL093017

Collier, J. C., & Bowman, K. P. (2004). Diurnal cycle of tropical precipitation in a general circulation model. *Journal of Geophysical Research*, *109*(D17), 2004JD004818. https://doi.org/10.1029/2004JD004818

Covey, C., Gleckler, P. J., Doutriaux, C., Williams, D. N., Dai, A., Fasullo, J., et al. (2016). Metrics for the diurnal cycle of precipitation: Toward routine benchmarks for climate models. *Journal of Climate*, *29*(12), 4461–4471. https://doi.org/10.1175/JCLI-D-15-0664.1

Crook, J., Klein, C., Folwell, S., Taylor, C. M., Parker, D. J., Stratton, R., & Stein, T. (2019). Assessment of the representation of West African storm lifecycles in convection-permitting simulations. *Earth and Space Science*, *6*(5), 818–835. https://doi.org/10.1029/2018EA000491

Dai, A. (2001). Global precipitation and thunderstorm frequencies. Part I: Seasonal and interannual variations. *Journal of Climate*, *14*(6), 1092–1111. https://doi.org/10.1175/1520-0442(2001)014<1092:GPATFP>2.0.CO;2

Dai, A. (2006). Precipitation characteristics in eighteen coupled climate models. *Journal of Climate*, *19*(18), 4605–4630. https://doi.org/10.1175/JCLI3884.1

Dai, A., Giorgi, F., & Trenberth, K. E. (1999). Observed and model-simulated diurnal cycles of precipitation over the contiguous United States. *Journal of Geophysical Research*, *104*(D6), 6377–6402. https://doi.org/10.1029/98JD02720

Dai, A., Lin, X., & Hsu, K.-L. (2007). The frequency, intensity, and diurnal cycle of precipitation in surface and satellite observations over low- and mid-latitudes. *Climate Dynamics*, *29*(7–8), 727–744. https://doi.org/10.1007/s00382-007-0260-y

Dennis, J., Fournier, A., Spotz, W. F., St-Cyr, A., Taylor, M. A., Thomas, S. J., & Tufo, H. (2005). High-resolution mesh convergence properties and parallel efficiency of a spectral element atmospheric dynamical core. *The International Journal of High Performance Computing Applications*, *19*(3), 225–235. https://doi.org/10.1177/1094342005056108

Dennis, J. M., Edwards, J., Evans, K. J., Guba, O., Lauritzen, P. H., Mirin, A. A., et al. (2012). CAM-SE: A scalable spectral element dynamical core for the community atmosphere model. *The International Journal of High Performance Computing Applications*, *26*(1), 74–89. https://doi.org/10.1177/1094342011428142

Donahue, A. S., Caldwell, P. M., Bertagna, L., Beydoun, H., Bogenschutz, P. A., Bradley, A. M., et al. (2024). To exascale and beyond—the Simple Cloud-Resolving E3SM Atmosphere Model (SCREAM), a performance portable global atmosphere model for cloud-resolving scales. *Journal of Advances in Modeling Earth Systems*, *16*(7), e2024MS004314. https://doi.org/10.1029/2024MS004314

Evans, K. J., Lauritzen, P. H., Mishra, S. K., Neale, R. B., Taylor, M. A., & Tribbia, J. J. (2013). AMIP simulation with the CAM4 spectral element dynamical core. *Journal of Climate*, *26*(3), 689–709. https://doi.org/10.1175/JCLI-D-11-00448.1

21698996, 2025, 20, Downloaded from https://agupubs.onlinelibrary.wiley.com/doi/10.1029/2025JD044113 by Youtong Zheng - University Of Houston Library , Wiley Online Library on [27/10/2025]. See the Terms and Conditions (https://onlinelibrary.wiley.com/terms-and-conditions) on Wiley Online Library for rules of use; OA articles are governed by the applicable Creative Commons License

Feng, Y.-C., Matthews, A., Rocque, M., Deng, M., Wendler, T., Johnson, K., et al. (2024). TRACER b1 data processing: Corrections, calibrations, and processing report. In *U.S. department of energy, atmospheric radiation measurement user facility*. DOE/SC-ARM-TR-297.

Feng, Z., Leung, L. R., Hardin, J., Terai, C. R., Song, F., & Caldwell, P. (2023). Mesoscale convective systems in DYAMOND global convection-permitting simulations. *Geophysical Research Letters*, *50*(4), e2022GL102603. https://doi.org/10.1029/2022GL102603

Freitas, S. R., Putman, W. M., Arnold, N. P., Adams, D. K., & Grell, G. A. (2020). Cascading toward a kilometer-scale GCM: Impacts of a scale-aware convection parameterization in the Goddard Earth observing system GCM. *Geophysical Research Letters*, *47*(17), e2020GL087682. https://doi.org/10.1029/2020GL087682

Gettelman, A., & Morrison, H. (2015). Advanced two-moment bulk microphysics for global models. Part I: Off-line tests and comparison with other schemes. *Journal of Climate*, *28*(3), 1268–1287. https://doi.org/10.1175/JCLI-D-14-00102.1

Golaz, J., Van Roekel, L. P., Zheng, X., Roberts, A. F., Wolfe, J. D., Lin, W., et al. (2022). The DOE E3SM model version 2: Overview of the physical model and initial model evaluation. *Journal of Advances in Modeling Earth Systems*, *14*(12), e2022MS003156. https://doi.org/10.1029/2022MS003156

Golaz, J.-C., Larson, V. E., & Cotton, W. R. (2002). A PDF-based model for boundary layer clouds. Part I: Method and model description. *Journal of the Atmospheric Sciences*, *59*(24), 3540–3551. https://doi.org/10.1175/1520-0469(2002)059<3540:APBMFB>2.0.CO;2

Heikenfeld, M., Marinescu, P. J., Christensen, M., Watson-Parris, D., Senf, F., Van Den Heever, S. C., & Stier, P. (2019). Tobac 1.2: Towards a flexible framework for tracking and analysis of clouds in diverse datasets. *Geoscientific Model Development*, *12*(11), 4551–4570. https://doi.org/10.5194/gmd-12-4551-2019

Iacono, M. J., Delamere, J. S., Mlawer, E. J., Shephard, M. W., Clough, S. A., & Collins, W. D. (2008). Radiative forcing by long-lived greenhouse gases: Calculations with the AER radiative transfer models. *Journal of Geophysical Research*, *113*(D13), 2008JD009944. https://doi.org/10.1029/2008JD009944

Jensen, M. (2019). Tracking Aerosol Convection Interactions ExpeRiment (TRACER) science plan. *No. BNL--212068-2019-INRE, 1561242; p. BNL--212068-2019-INRE, 1561242)*. https://doi.org/10.2172/1561242

Judt, F. (2018). Insights into atmospheric predictability through global convection-permitting model simulations. *Journal of the Atmospheric Sciences*, *75*(5), 1477–1497. https://doi.org/10.1175/JAS-D-17-0343.1

Kousky, V. E. (1980). Diurnal rainfall variation in northeast Brazil. *Monthly Weather Review*, *108*(4), 488–498. https://doi.org/10.1175/1520-0493(1980)108<0488:DRVINB>2.0.CO;2

Lee, Y.-C., & Wang, Y.-C. (2021). Evaluating diurnal rainfall signal performance from CMIP5 to CMIP6. *Journal of Climate*, *34*(18), 7607–7623. https://doi.org/10.1175/JCLI-D-20-0812.1

Ma, H., Klein, S. A., Lee, J., Ahn, M., Tao, C., & Gleckler, P. J. (2022). Superior daily and sub-daily precipitation statistics for intense and long-lived storms in global storm-resolving models. *Geophysical Research Letters*, *49*(8), e2021GL096759. https://doi.org/10.1029/2021GL096759

Matsuno, T. (2016). Prologue: Tropical meteorology 1960–2010—Personal recollections. *Meteorological Monographs*, *56*, vii–xv. https://doi.org/10.1175/AMSMONOGRAPHS-D-15-0012.1

Merlis, T. M., Cheng, K.-Y., Guendelman, I., Harris, L., Bretherton, C. S., Bolot, M., et al. (2024). Climate sensitivity and relative humidity changes in global storm-resolving model simulations of climate change. *Science Advances*, *10*(26), eadn5217. https://doi.org/10.1126/sciadv.adn5217

Morrison, H., & Milbrandt, J. A. (2015). Parameterization of cloud microphysics based on the prediction of bulk ice particle properties. Part I: Scheme description and idealized tests. *Journal of the Atmospheric Sciences*, *72*(1), 287–311. https://doi.org/10.1175/JAS-D-14-0065.1

Muller, C. J., & Held, I. M. (2012). Detailed investigation of the self-aggregation of convection in cloud-resolving simulations. *Journal of the Atmospheric Sciences*, *69*(8), 2551–2565. https://doi.org/10.1175/JAS-D-11-0257.1

Oware, R. K. T. (2025). Evaluating E3SM global storm-resolving model simulations of deep convection: Insights from DP-SCREAM during TRACER [Dataset]. *Zenodo*. https://doi.org/10.5281/ZENODO.15271730

Pincus, R., Mlawer, E. J., & Delamere, J. S. (2019). Balancing accuracy, efficiency, and flexibility in radiation calculations for dynamical models. *Journal of Advances in Modeling Earth Systems*, *11*(10), 3074–3089. https://doi.org/10.1029/2019MS001621

Randall, D., Khairoutdinov, M., Arakawa, A., & Grabowski, W. (2003). Breaking the cloud parameterization deadlock. *Bulletin of the American Meteorological Society*, *84*(11), 1547–1564. https://doi.org/10.1175/BAMS-84-11-1547

Rasch, P. J., Xie, S., Ma, P.-L., Lin, W., Wang, H., Tang, Q., et al. (2019). An overview of the atmospheric component of the energy exascale Earth system model. *Journal of Advances in Modeling Earth Systems*, *11*(8), 2377–2411. https://doi.org/10.1029/2019MS001629

Rio, C., Hourdin, F., Grandpeix, J.-Y., & Lafore, J.-P. (2009). Shifting the diurnal cycle of parameterized deep convection over land. *Geophysical Research Letters*, *36*(7), 2008GL036779. https://doi.org/10.1029/2008GL036779

Satoh, M., Matsuno, T., Tomita, H., Miura, H., Nasuno, T., & Iga, S. (2008). Nonhydrostatic Icosahedral Atmospheric Model (NICAM) for global cloud resolving simulations. *Journal of Computational Physics*, *227*(7), 3486–3514. https://doi.org/10.1016/j.jcp.2007.02.006

Satoh, M., Stevens, B., Judt, F., Khairoutdinov, M., Lin, S.-J., Putman, W. M., & Düben, P. (2019). Global cloud-resolving models. *Current Climate Change Reports*, *5*(3), 172–184. https://doi.org/10.1007/s40641-019-00131-0

Satoh, M., Tomita, H., Yashiro, H., Miura, H., Kodama, C., Seiki, T., et al. (2014). The non-hydrostatic icosahedral atmospheric model: Description and development. *Progress in Earth and Planetary Science*, *1*(1), 18. https://doi.org/10.1186/s40645-014-0018-1

Silvestri, L., Saraceni, M., & Bongioannini Cerlini, P. (2024). Numerical diffusion and turbulent mixing in convective self-aggregation. *Journal of Advances in Modeling Earth Systems*, *16*(5), e2023MS004151. https://doi.org/10.1029/2023MS004151

Sokolowsky, G. A., Freeman, S. W., Jones, W. K., Kukulies, J., Senf, F., Marinescu, P. J., et al. (2023). Tobac v1.5: Introducing fast 3D tracking, splits and mergers, and other enhancements for identifying and analysing meteorological phenomena. *Atmospheric Sciences*. https://doi.org/10.5194/egusphere-2023-1722

Song, J., Song, F., Feng, Z., Leung, L. R., Li, C., & Wu, L. (2024). Realistic precipitation diurnal cycle in global convection-permitting models by resolving mesoscale convective systems. *Geophysical Research Letters*, *51*(13), e2024GL109945. https://doi.org/10.1029/2024GL109945

Stevens, B., & Bony, S. (2013). What are climate models missing? *Science*, *340*(6136), 1053–1054. https://doi.org/10.1126/science.1237554

Stevens, B., Satoh, M., Auger, L., Biercamp, J., Bretherton, C. S., Chen, X., et al. (2019). DYAMOND: The DYnamics of the atmospheric general circulation modeled on non-hydrostatic domains. *Progress in Earth and Planetary Science*, *6*(1), 61. https://doi.org/10.1186/s40645-019-0304-z

Su, T., Zhang, Y., & Tian, J. (2025). Boundary-layer-coupled and decoupled clouds in global storm-resolving models: Comparisons with the ARM observations. *Journal of Geophysical Research: Atmospheres*, *130*(5), e2024JD041915. https://doi.org/10.1029/2024JD041915

Takasuka, D., Satoh, M., Miyakawa, T., Kodama, C., Klocke, D., Stevens, B., et al. (2024). A protocol and analysis of year-long simulations of global storm-resolving models and beyond. *Review*. https://doi.org/10.21203/rs.3.rs-4458164/v1

21698996, 2025, 20, Downloaded from https://agupubs.onlinelibrary.wiley.com/doi/10.1029/2025JD044113 by Youtong Zheng - University Of Houston Library , Wiley Online Library on [27/10/2025]. See the Terms and Conditions (https://onlinelibrary.wiley.com/terms-and-conditions) on Wiley Online Library for rules of use; OA articles are governed by the applicable Creative Commons License

Tang, S., Gleckler, P., Xie, S., Lee, J., Ahn, M.-S., Covey, C., & Zhang, C. (2021). Evaluating the diurnal and semidiurnal cycle of precipitation in CMIP6 models using Satellite- and ground-based observations. *Journal of Climate*, *34*(8), 3189–3210. https://doi.org/10.1175/JCLI-D-20-0639.1

Tang, S., Tao, C., Xie, S., & Zhang, M. (2019). Description of the ARM large-scale forcing data from the constrained variational analysis (VARANAL) version 2. *DOE Office of Science Atmospheric Radiation Measurement (ARM) Program (United States)*. https://doi.org/10.2172/1546995

Tao, C., Xie, S., Ma, H., Bechtold, P., Cui, Z., Vaillancourt, P. A., et al. (2024). Diurnal cycle of precipitation over the tropics and central United States: Intercomparison of general circulation models. *Quarterly Journal of the Royal Meteorological Society*, *150*(759), 911–936. https://doi.org/10.1002/qj.4629

Tian, J., Zhang, Y., Klein, S. A., Terai, C. R., Caldwell, P. M., Beydoun, H., et al. (2024). How well does the DOE global storm resolving model simulate clouds and precipitation over the Amazon? *Geophysical Research Letters*, *51*(14), e2023GL108113. https://doi.org/10.1029/2023GL108113

Tian, Y., Zhang, Y., Klein, S. A., & Schumacher, C. (2021). Interpreting the diurnal cycle of clouds and precipitation in the ARM Go Amazon observations: Shallow to deep convection transition. *Journal of Geophysical Research: Atmospheres*, *126*(5), e2020JD033766. https://doi.org/10.1029/2020JD033766

Tomita, H., Miura, H., Iga, S., Nasuno, T., & Satoh, M. (2005). A global cloud-resolving simulation: Preliminary results from an aqua planet experiment. *Geophysical Research Letters*, *32*(8), 2005GL022459. https://doi.org/10.1029/2005GL022459

Tompkins, A. M., & Semie, A. G. (2017). Organization of tropical convection in low vertical wind shears: Role of updraft entrainment. *Journal of Advances in Modeling Earth Systems*, *9*(2), 1046–1068. https://doi.org/10.1002/2016MS000802

Tuftedal, K. S., Treserras, B. P., Oue, M., & Kollias, P. (2024). Shallow- and deep-convection characteristics in the greater Houston, Texas, area using cell tracking methodology. *Atmospheric Chemistry and Physics*, *24*(9), 5637–5657. https://doi.org/10.5194/acp-24-5637-2024

Wang, D., Melvin, E. C., Smith, N., Jensen, M. P., Gupta, S., Abdullah-Smoot, A., et al. (2024). TRACER perspectives on gulf-breeze and bay-breeze circulations and coastal convection. *Monthly Weather Review*, *152*(10), 2207–2228. https://doi.org/10.1175/MWR-D-23-0292.1

Watters, D., Battaglia, A., & Allan, R. P. (2021). The diurnal cycle of precipitation according to multiple decades of global satellite observations, three CMIP6 models, and the ECMWF reanalysis. *Journal of Climate*, *34*(12), 5063–5080. https://doi.org/10.1175/JCLI-D-20-0966.1

Widener, K., Bharadwaj, N., & Johnson, K. (2012). Ka-Band ARM Zenith Radar (KAZR) instrument handbook. *DOEARM*. https://doi.org/10.2172/1035855

Xie, S., Cederwall, R. T., & Zhang, M. (2004). Developing long-term single-column model/cloud system–resolving model forcing data using numerical weather prediction products constrained by surface and top of the atmosphere observations. *Journal of Geophysical Research*, *109*(D1), 2003JD004045. https://doi.org/10.1029/2003JD004045

Xie, S., Lin, W., Rasch, P. J., Ma, P., Neale, R., Larson, V. E., et al. (2018). Understanding cloud and convective characteristics in version 1 of the E3SM atmosphere model. *Journal of Advances in Modeling Earth Systems*, *10*(10), 2618–2644. https://doi.org/10.1029/2018MS001350

Xie, S., McCoy, R. B., Klein, S. A., Cederwall, R. T., Wiscombe, W. J., Jensen, M. P., et al. (2010). Clouds and more: ARM climate modeling best estimate data: A new data product for climate studies. *Bulletin of the American Meteorological Society*, *91*(1), 13–20. https://doi.org/10.1175/2009BAMS2891.1

Xie, S., & Tao, C. (2021). 60v1varanaecmwf (c1) (1993354) [Dataset]. *Atmospheric Radiation Measurement (ARM) Archive, Oak Ridge National Laboratory (ORNL), Oak Ridge, TN (US); ARM Data Center, Oak Ridge National Laboratory (ORNL)*. https://doi.org/10.5439/1993354

Xie, S., Wang, Y., Lin, W., Ma, H., Tang, Q., Tang, S., et al. (2019). Improved diurnal cycle of precipitation in E3SM with a revised convective triggering function. *Journal of Advances in Modeling Earth Systems*, *11*(7), 2290–2310. https://doi.org/10.1029/2019MS001702

Zhang, G. J., & McFarlane, N. A. (1995). Sensitivity of climate simulations to the parameterization of cumulus convection in the Canadian climate centre general circulation model. *Atmosphere-Ocean*, *33*(3), 407–446. https://doi.org/10.1080/07055900.1995.9649539

Zhang, J., Bogenschutz, P., Tang, Q., Cameron-smith, P., & Zhang, C. (2024). Leveraging regional mesh refinement to simulate future climate projections for California using the simplified convection-permitting E3SM atmosphere model version 0. *Geoscientific Model Development*, *17*(9), 3687–3731. https://doi.org/10.5194/gmd-17-3687-2024

Zhang, J., Howard, K., Langston, C., Kaney, B., Qi, Y., Tang, L., et al. (2016). Multi-Radar Multi-Sensor (MRMS) quantitative precipitation estimation: Initial operating capabilities. *Bulletin of the American Meteorological Society*, *97*(4), 621–638. https://doi.org/10.1175/BAMS-D-14-00174.1

Zhang, M. H., Lin, J. L., Cederwall, R. T., Yio, J. J., & Xie, S. C. (2001). Objective analysis of ARM IOP data: Method and sensitivity. *Monthly Weather Review*, *129*(2), 295–311. https://doi.org/10.1175/1520-0493(2001)129<0295:OAOAID>2.0.CO;2

Zheng, X., Zhang, Y., Klein, S. A., Zhang, M., Zhang, Z., Deng, M., et al. (2024). Using satellite and ARM observations to evaluate cold air outbreak cloud transitions in E3SM global storm-resolving simulations. *Geophysical Research Letters*, *51*(8), e2024GL109175. https://doi.org/10.1029/2024GL109175

21698996, 2025, 20, Downloaded from https://agupubs.onlinelibrary.wiley.com/doi/10.1029/2025JD044113 by Youtong Zheng - University Of Houston Library , Wiley Online Library on [27/10/2025]. See the Terms and Conditions (https://onlinelibrary.wiley.com/terms-and-conditions) on Wiley Online Library for rules of use; OA articles are governed by the applicable Creative Commons License